AEROFAST: DEVELOPMENT OF CORK TPS MATERIAL AND A 3D COMPARATIVE THERMAL/ABLATION ANALYSIS OF AN APOLLO & A BICONIC SLED SHAPE FOR AN AEROCAPTURE MISSION

G. Pinaud[†], A.J. van Eekelen[*], and J.-M. Bouilly[†]

[†] ASTRIUM-SAS, *F-33165 St. Médard-en-Jalles, France, E-mail: Gregory.Pinaud@astrium.eads.net, Jean-Marc.Bouilly@astrium.eads.net*

[*] SAMTECH *s.a., B-4031 Angleur-Liège, Belgium, E-mail: Tom.vanEekelen@samtech.com*

ABSTRACT

An Aerocapture vehicle travelling from Earth to Mars approaches that planet on a hyperbolic interplanetary trajectory. Upon arrival, the vehicle will perform a single atmospheric pass to significantly reduce its speed, and enters into an orbit around the planet. This manoeuvre uses aerodynamic drag instead of propulsion for orbit insertion, and potentially leads to large mass (fuel) savings as well as reduced flight times (higher arrival speed). However, Aerocapture results in significant aerodynamic heating, necessitating a Thermal Protection System (TPS), as well as the use of a guidance system to assure that the spacecraft leaves the planetary atmosphere on the correct trajectory. In the frame of the seventh European Community Framework Program (FP7), the AEROFAST (AEROcapture for Future space tranSporTation) research and development project aims at preparing a demonstration of a Martian Aerocapture mission and increasing the Technology Readiness Level (TRL).

One of the aims of this paper, is to present the development of an innovative cork based material and the selection process of the different formulations. The material must be able to withstand the severe front shield aerothermal environment. Numerous formulations have been investigated using a parametric combination of cork granule size, resin type/ratio, reinforcement fraction, fillers and the mixing and agglomeration processes. A basic (thermo-mechanical) characterization and qualitative analysis allowed for a first selection of the 4 most promising candidates. These candidates are being tested in the inductive plasma wind-tunnel facilities (COMETE) of ASTRIUM. These tests are performed in a stagnation point configuration, for an aerothermal environment similar to the AEROFAST aerocapture mission.

In parallel, a 3D ablation and charring material model has been implemented in the finite element program SAMCEF, and successfully validated during the AEROFAST project. The numerical model consists of three sets of equations, namely the transient heat balance equation, the steady state mass balance equation and the charring equations. For the charring of the material we use a multi-species Arrhenius model with the species densities as degrees of freedom. The ablation is modelled by a surface imposed and temperature dependent ablation speed, followed by an in volume mesh deformation. Two main probe aerodynamic shapes and concepts have been evaluated, namely an Apollo like shape and a biconic sled with a characteristic diameter of 4 m. A thermo-mechanical comparative analysis of the front-shield has been carried out. The space probes are made of Norcoat-Liège (a low density phenolic resin impregnated cork material) which will serve as a baseline solution. The 3D heat load history (convective and radiative), over the front-shield, is based on the maximum energy trajectory extracted from a statistical Monte Carlo GNC study for a CO_2 Martian atmosphere.

Preliminary experimental plasma tests demonstrate promising enhanced thermal and ablative properties and also the need to improve numerical response model.

1. INTRODUCTION

Aerocapture is an interesting technology for Solar System exploration that aim at decelerating the spacecraft through a single pass in a planetary atmosphere and consequently at achieving a targeted orbit. This manoeuvre saves a significant amount of propellant with regard to a more conventional insertion technique. Aerocapture its a multidisciplinary technique involving various field such as system analysis and integrated vehicle design, aerodynamics, aero-thermal environments, thermal protection systems (TPS), guidance, navigation and control (GN&C), instrumentation; each of them being strongly linked and playing a key role in the success of a challenging mission. Currently, Europe doesnt demonstrate a sufficient Technology Readiness Level (TRL) of aerocapture technology mainly because of its little experience while a TRL 6 is mandatory to envisage aerocapture technology for operational missions. Funded under the 7^{th} Framework Program (FP7) of the European Community, the AEROFAST project has the ambition to remediate to

these lacks and is dedicated to increase the TRL level of aero-capture technology up to level 4 through a complete mission study of a Martian aero-capture. The main 5 objectives of the project are (see [1]):

- **OBJ1:** Define a project of aero-capture demonstration
- **OBJ2:** Make a significant progress in space transportation by increasing the TRL of the planetary relative navigation and the aerocapture algorithm up to 5
- **OBJ3:** Build a breadboard to test in real time the pre-aerocapture and aerocapture GNC algorithms
- **OBJ4:** Demonstrate/prototype the thermal protection system for such a mission
- **OBJ5:** Define on-board instrumentation for aero-capture phase recovery

The present paper focus on the objective 4 by describing the approach and the preliminary results of the development of an innovative cork based thermal protection material compliant with the specific mission requirement. The development of the 3D charring ablation module (Amaryllis) in the finite element code SAMCEF was also a major breakthrough for the project and the sizing activities. At the beginning of the project, the choice of the aero- shape was open. After a trade off between an Apollo like shape and a truncated sphero-biconic shape to name but a few, considering various criteria such as volume, mass, dynamic stability, lift over drag ratio, innovation, the selection was on favor of the biconic shape. Thus, the present paper relates also on the heat front shield thermal 3D sizing and a design comparison between these two latest shapes.

2. EXISTING CORK THERMAL PROTECTION MATERIAL

As objective 4 of AEROFAST project is to demonstrate and prototype a thermal protection for an aero-capture mission, the 2 main leaders of the TPS work package (ASTRIUM and AMORIM) naturally proposed their top cork product as baseline: respectively Norcoat-Liège for ASTRIUM (AST) and TP45-50 for AMORIM CORK COMPOSITE (ACC). During the material screening phase of the project other cork composite producers have been identified such as Lockheed Martin, NASA, ARA, MSFC to name but a few. However, this paper will focus only on the cork products family of AST and ACC.

2.1. Norcoat-Liège

Norcoat-Liège is low density insulators based on cork granules and phenolic resin as matrix manufactured by Lièges-HPK Company (Lavardac, 47230 France) and marketed by ASTRIUM Space Transportation an EADS company. ASTRIUM has a long experience in the use of Norcoat-Liège since 40 years. Indeed, Norcoat-Liège is currently use on ARIANE5 launcher and on M51 French deterrence force missile. This material has also been successfully used on ARD back cover (Atmospheric Reentry Demonstrator) or on the front heat shield of the BEAGLE2 probe for the European MARS EXPRESS mission to MARS.

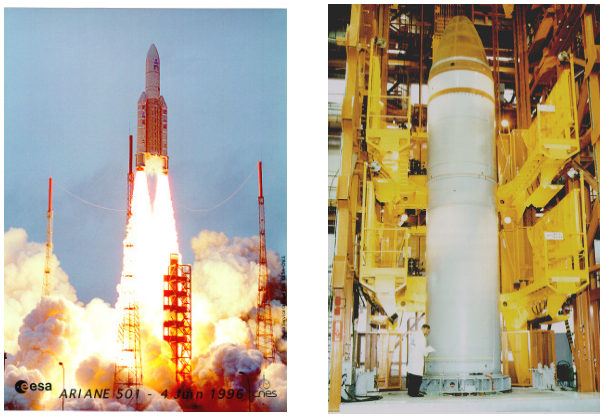

Figure 1. Norcoat-Liège on ARIANE5 and French deterrence force missile

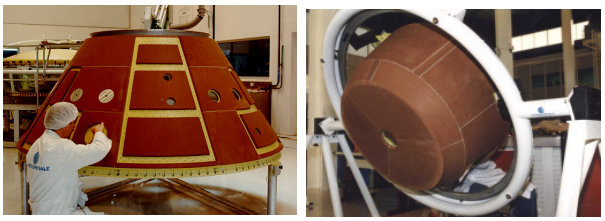

Figure 2. Norcoat-Liège on ARD (Atmospheric re-entry Demonstrator) back cover.

Figure 3. Norcoat-Liège tiles bonding process front heat shield and back cover of Beagle2 probe.

Norcoat-Liège is produced under the form of flat plat of various thicknesses from 1.5 to 19 mm. A brief summary of possible process is described hereunder:

- Cutting

- Machining
- Hot press forming
- Bonding under pressure on the equipment
- Possibility of outgassing treatment for space applications
- Applicable on developable or not very complex surfaces

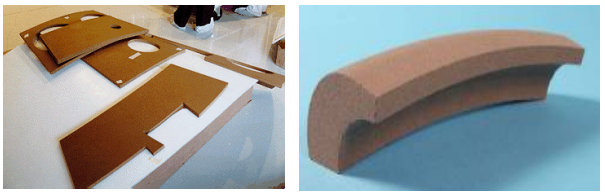

Figure 4. Norcoat-Liège manufacturing process.

There are three material variations:

- Norcoat HPK - standard material with no agents
- Norcoat HPK FI - with fungicide agent (F) and a fire-proof agent (I) which confers self-extinguishing properties.
- Norcoat HPK FIH - with fungicide agent (F); a fire-proof agent (I) which confers self-extinguishing and a damp-proof agent (H) which limits water absorption in the material.

The properties of the Norcoat-Liège HPK FIH, are given in Table 1. For planetary exploration mission space grade

Table 1. Main properties of the Norcoat-Liège HPK FIH

Property	Units	Value
Density	kg/m^3	470
Tensile Strength	Mpa	2.5
Elongation at break	%	6
Thermal conductivity (150°)	W/(m.K)	0.08
Specific heat (150°)	kJ/(kg.K)	2.4

Norcoat-Liège is also available with planetary protection assembly constraints being taken into account. For NETLANDER, MARS EXPRESS and EXOMARS mission ASTRIUM Simoun arc jet facility enable the qualification of the Norcoat-Liège material under CO_2 atmosphere. Systematic study of the thermal and ablative behavior is carried out in the framework of various programs and under various environment from low temperature heating blanket, infra red furnace, to inductive and arc jet plasma environment leading to a robust thermochemical and mechanical numerical model. This numerical model is currently applied for EXOMARS heat shield sizing activities associated with specific margin policy.

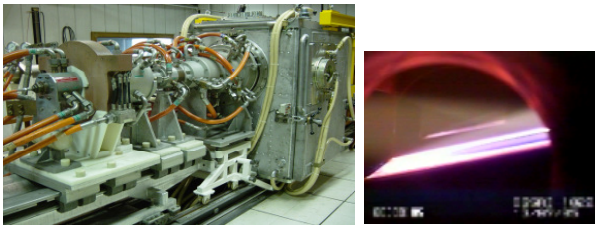

Figure 5. Simoun 9 MW arc jet test facility

2.2. TP45-50

With the cork granules, ACC produces two cork composites especially for the space sector, the P45 and the P50, with different densities and properties. The two cork composites described are composed with high cork content (more than 70 percent in weight) and a thermoset binder. The cork raw material is composed of uniformly ground cork of the lowest density and cleanness, with controlled sizes. The binder system accounts for more than 20 percent of the weight and is composed of a thermosetting phenolic resin with polyol plasticizer, exclusively used on these materials. The mixing and curing procedures are based on existing methodology and equipment. Blocks of cork are produced by mixing the cork and binder, compressing and moulding the slurry, then curing with heat and time. The blocks are then cut according the required thickness into flexible sheets. The P45 cork sheets are produced using 10/20 Cork granules obtaining a low density agglomerate. The sheets could be delivered in several thicknesses (from 0.8 mm till 125 mm) and with a maximum width and length of 700 $\times$ 1250 mm, respectively. P50 is produced using 20/40 cork granules and different ratios of resin and cork along with variation of the compression ratios during moulding, obtaining a medium density agglomerated cork sheet. The P50 basic properties are given in Table 2.

Table 2. Main properties of the P45 ACC cork based TP material

Property	Units	Value
Density	kg/m^3	Max 512
Tensile Strength	Mpa	Min 1.72 2.5
Elongation at break	%	13
Thermal conductivity (150°)	W/(m.K)	0.07
Specific heat (150°)	kJ/(kg.K)	2.1

The P45 and P50 are mainly use for thermal protection on the solid rocket booster (SRB) of the space Shuttle as well as on the Delta rochets for these various locations and thermal and mechanical environment:

- Booster nose cone
- frustum bolt catcher

- external skirt insulation

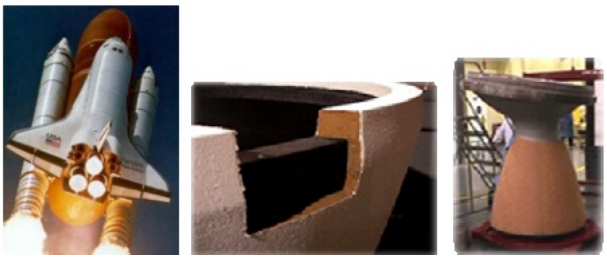

Figure 6. P45 on SRB of the Space Shuttle and P50 on the Delta Rockets

Among the 2 well known candidates seen as the state of art for cork based thermal protection material none were optimized for the specific characteristics of a Martian aerocapture mission. Thats why, AEROFAST project is the opportunity to gather the know-how and the experience of the AST and ACC and benefit of this synergy to pave the way for the development of an optimized material for such aerocapture mission and more generally to elaborate an innovative and improve family of cork based material.

3. MATERIAL DEVELOPMENT STRATEGY

A preliminary phase drew the baseline of the aerocapture project and more specifically the aerocapture phase thermal and mechanical environment. The TPS requirements (see [2]) were identified as well as the improvement needs. Consequently within the aerocapture specific range of maximum heat flux and heat load the targeted new cork based material family properties would be:

- an optimized lowest density
- a better thermal insulation efficiency
- a better resistance to erosion and a lowest fragility of the charred layer
- the smoothest possible charred wall
- a predictive swelling phenomena

Because of the more severe environment meet on the front-shield in comparison with the back cover, 2 cork based material families will be developed:

- a reinforced material which can withstand stagnation like environment
- a superlight material for very low heat flux and mechanical load for aft side and leeward side.

A two step iterative process is adopted in order to select the best formulations. During a first loop, basic and elementary thermal and mechanical properties of the new materials are measured to realize a preliminary selection. Based on this pre-selection deeper analysis are perform (extended thermal properties, plasma test...) The trade-off criteria are consistent with the targeted properties of the new material and are listed hereunder:

- mass loss
- thickness recession
- charred material integrity
- cracks number, thickness and depth

In parallel non ablative (non cork) solutions have been introduced in the global trade off in order to balance and compare the advantages and drawbacks of both family (ablative and non ablative). Finally, the strategy can be summarized in Fig. 7.

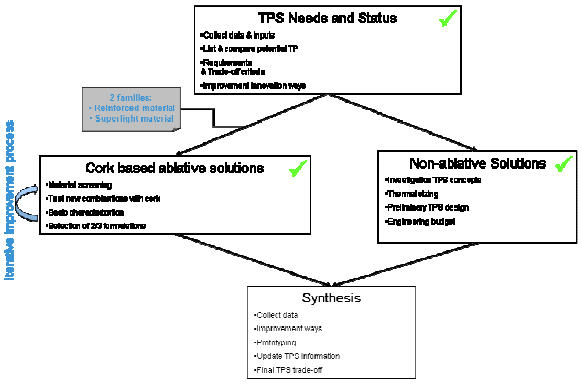

Figure 7. Material development strategy diagram

4. ABLATIVE SOLUTION

4.1. Innovation Road Map

Based on the generally contradictory requirements, some innovation ways were proposed and investigated to improve existing cork ablative material. Fig. 8 presents the different ways explored that lead to the elaboration of more than 25 formulations:

- In order to improve the cork based material behavior with regard to ablation, reinforcement such as carbon and basalt fibers were investigated. The initial amount and length of the fibers were set thanks to previous ASTRIUM in-house experience.

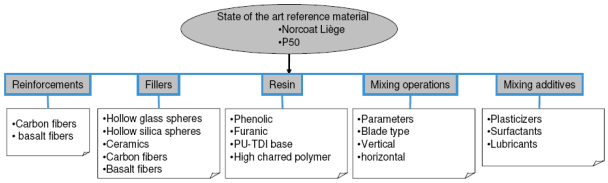

Figure 8. Innovation ways for cork based materials

- Fillers like hollow glass, silica spheres, ceramics, carbon and basalt fibers were considered in order to modify density and thermal behavior.
- 2 main synthetic resins (phenolic and furanic) were mix to cork granules in various amounts. - The mixing operations such as blade type, orientation and speed seemed to play an important role to get as most as possible an homogenous material.
- To improve the efficiency of the mixing operations, different plasticizers, surfactants and lubricants were also tested.

Based on this development roadmap, more than 25 different formulations were elaborated and are depicted in the Fig. 9. Since it was unrealistic to perform full thermal and

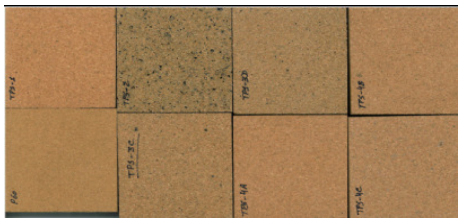

Figure 9. Sample of new cork formulations before preselection

mechanical characterizations, only basics measurements have been performed. These basic, quick and relatively cheap characterizations consist of:

- Low heating rate thermogravimetric analysis (TGA)
- Thermomechanic analysis (TMA)
- Reaction to fire and cone calorimeter test (ISO 5660-1)
- Hardness
- Tensile strength
- Elongation
- Compression/recovery
- Flexibility

Figure 10. Example of material basic characterizations by cone calorimeter

4.2. Selection of the Most Promising Formulations

Once the most promising formulations being pre- selected, deeper thermochemical analyses were performed with special focus on:

- thermal conductivity at room temperature to 200 °C
- specific heat from -123° to 177° C by differential scanning calorimeter (DSC)
- thermogravimetric analysis with heating rate from 5 K to 100 K per minute at room temperature until 1000 °C

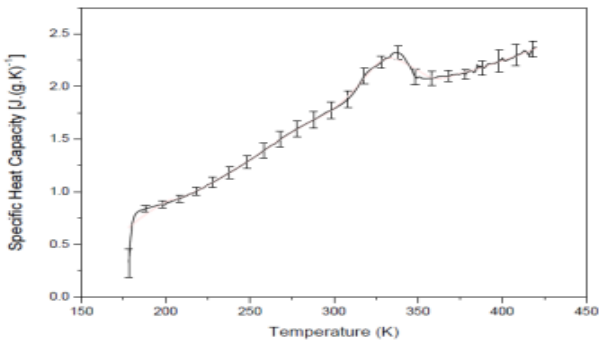

Figure 11. Specific heat measurements by DSC

4.3. Plasma Test Campaign

Finally, among the initial set of 25 formulations, the selection process sort out 4 candidates who potentially fulfilled the front heatshield requirements and preliminary criteria, and 3 candidates for the back cover and leeward side environment. A plasma test campaign has been carried out on the 4 more promising front heat shield candidates to asses their thermal and ablative behavior under realistic aerocapture environment. Thus, the ground test thermal environments have been set on the basis of the simulated flight conditions for the sizing trajectory

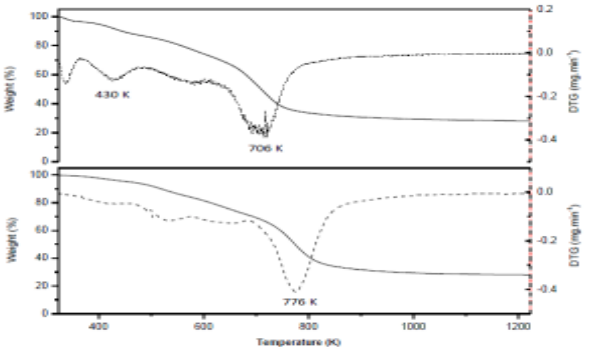

Figure 12. Comparison of thermogravimetric analysis at 2 different heating rates

(maximum heat load). Aertothermal Navier Stokes CFD simulations as well as radiative Monte Carlo simulations have been performed by ONERA (France) to assess heat flux wall distribution (at maximum dynamic pressure and at pick heat flux) on the selected truncated biconic shape in order to validate and to scale semi-empiric ASTRIUM correlation. As the biconic aero-shape presents huge vari-

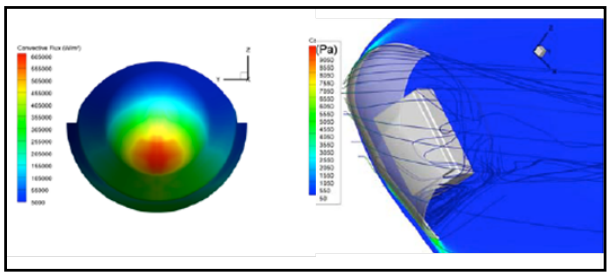

Figure 13. Convective heat flux distribution at pick heat flux and satellite-flow interaction

ation of flux along its profile 2 missions were proposed. The proposed values are also consistent with the lower level of flux met on the previous Apollo like shape studied during the project. Among the panel of plasma test facility operated in ASTRIUM, the COMETE (75 kW) inductive torch has been selected. Indeed, in a stagnation point configuration, heat flux from 150 to 3000 kW/m^2 can be reach under 30 to 900 mbar AIR pressure. Finally, the experimental heat flux history is adapted to the ground test facility capability, for which the minimum stabilized heat flux is around 150 kW/m^2.

In Fig. 16 we compare the ground experimental mission with the flight conditions for the 2 defined missions (Biconic 1, Biconic 2): The heat flux level is selected to enable a proper analysis of key phenomena such as pyrolysis or ablation. The test duration is determined so that heat load is of the same order of magnitude than during flight. The representativity of the ground test campaign in terms of heat flux and energy is shown in Table 3. Tests will be carried out in AIR because operability

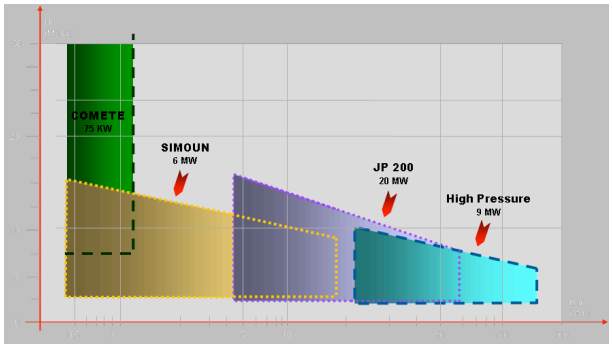

Figure 14. ASTRIUM plasma test facilities and operating field

Figure 15. COMETE plasma test facility at ASTRIUM

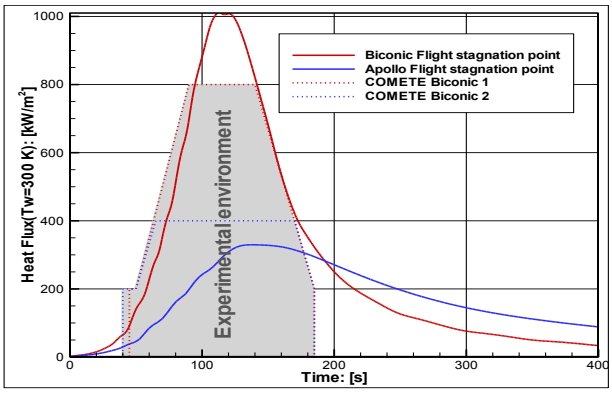

Figure 16. Comparison of flight and ground experimental conditions in COMETE facility

Table 3. Representativity assessment of the plasma test

	Biconic sled		Apollo like shape	
	Flight	Ground mision 1	Flight	Ground mission 2
Max heat flux (kW/m^2)	1011	800	330	400
Max heat load (MJ/m^2)	114	84	92	53

of COMETE facility in CO_2 (Martian like atmosphere) is not yet demonstrated. Previous ASTRIUM comparative plasma test carried out in CO_2 and in AIR atmosphere on Norcoat-Liège have always shown similar results. The pressure will stay at a constant value around 100 mbar which is the maximum expected flight condition at pick heat flux.

The samples will have a cylindrical shape with a diameter of 50 mm and a useful thickness of 20 mm. Each material piece will be instrumented with one thermocouple on the back face. Since theses test are not devoted to

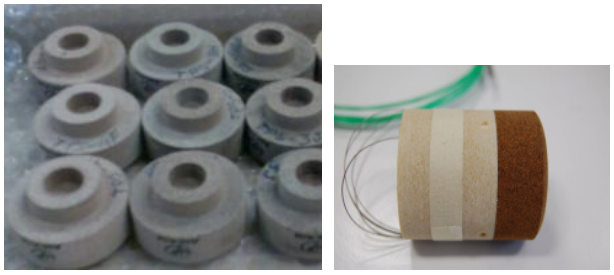

Figure 17. Sample definition and instrumentation

material qualification, only comparative analysis will be performed. Tests are currently being processed and the synthesis phase will start in the coming weeks. The first selected formulations tested already show improved performance considering ablation and surface roughness for the lowest level flux mission (Biconic 2):

Figure 18. After test comparison of surface visual aspect between P50 and TPS3J (carbon fibers reinforced cork based material)

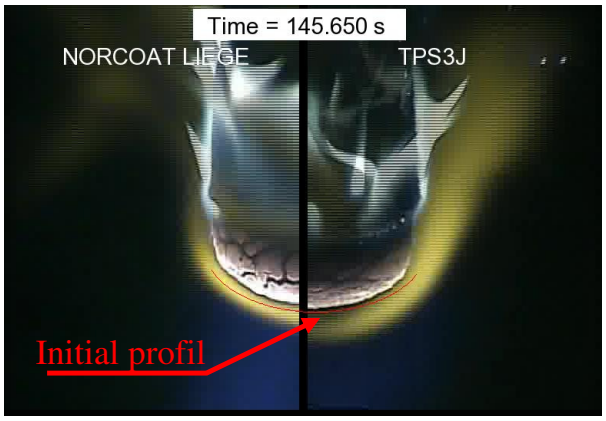

Figure 19. Initial and ablated profile on the mission Biconic 2 for Norcoat-Liège and TPS3J reinforced material

5. NON-ABLATIVE SOLUTION

Mainly, two non ablative solutions were proposed namely CMC and FEI and will be included in the final trade-off of material, the heat shield sizing and mass budget being realized.

5.1. CMC

The CMC material (Ceramic Matrix Composite) is typically a windward side fiber reinforced ceramic TPS that is made of carbon-reinforced silicon carbide (C/SiC). C/SiC combines the strength and stiffness of carbon fibers with a more oxidation resistant matrix. Between the CMC and the substructure an high temperature micro-fiber insulation is integrated therefore metallic or ceramic stand-offs will be used to fix the CMC tile to the vehicle structure. All along the piece perimeter, a sealing system is applied protecting the gap to neighbouring panels of the same material or adjacent structures. This material has been qualified for X38 vehicle:

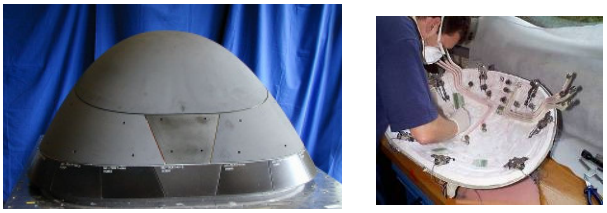

Figure 20. CMC nose tile and assembling process on X38

5.2. FEI

The product family of FEI types has been established in recent years covering the range of temperatures from 300 °C to 1100 °C developed and commercialized by ASTRIUM-EADS. The FEI types are made from different organic and inorganic fibers components like felts, fabrics and threads. The materials used are NOMEX®, KEVLAR®, PBI, silica, alumina and ABS ceramic according to the required temperature range. In general FEI's are quilted blankets composed of a felt which is enclosed by an inner and outer fabric and sewn together by threads. Various coatings are available to stiffen the other surface and to provide certain thermo-optical properties. Water repellents can be applied to minimize the hygroscopic behavior. The FEI blanket is usually glued with an RTV adhesive to the substructure of the vehicle. FEI blankets have already flown on ARD back cover and were also qualified on X38.

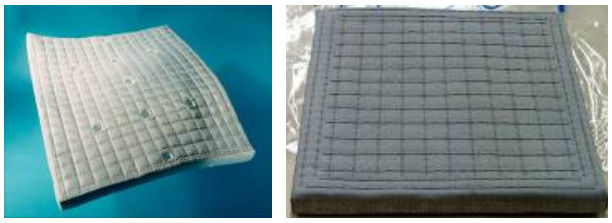

Figure 21. Typical FEI Blankets

6. VEHICLE DESIGN

6.1. Aerocapture Trajectory

The nominal aerocapture trajectory has been computed in order to guaranty a trajectory after aerocapture compliant w.r.t. the final orbit expected. The feasibility of the aerocapture is mainly driven by the condition at the EIP. The aerocapture corridor is bounded by extreme over-shoot and under-shoot trajectories. The width of the corridor leads to maximum FPA errors at entry point below $\pm 1.24°$.

Table 4. Entry corridor for aerocapture at Mars arrival

Entry Interface Points (EIP) at 120 km AGL	
Relative velocity	6377.6 m/s
Flight Path Angle	-10.33°

6.2. Aeroshape Trade-off

Aerocapture requires an Aeroshape that provides a lift-over-drag (L/D) ratio with sufficient provision (L/D $>$ 0.3) and sufficient static stability performances. In addition, the aeroshape must protect the payloads (P/L) from the severe aero-thermal environment during the aerocapture, and shall be safely jettison able at the beginning of the pre-A/C phase. In the frame of Aerofast, a trade-off has been performed considering two configurations:

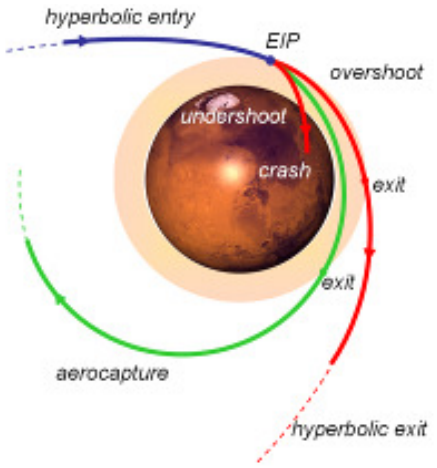

Figure 22. Aerocapture trajectory problematic

- A blunt body capsule derived from Apollo, ARD concepts
- A lifting body dealing with bi-conic shape.

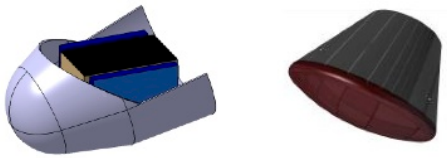

Figure 23. Final aero-shape trade-off.

By considering L/D requirements, payload protection w.r.t. aerothermal heating and layout constraints, the bi-conic shape has been selected.

6.3. Aerothermodynamics

Aerodynamic, aerothermodynamic and radiative environment on the biconic shape have been assessed for different angle of attack and at key points on the trajectories. Heat fluxes histories have been assessed along two worst case aerocapture trajectories identified by Monte Carlo analysis (see [3]):

- overshoot trajectory corresponding to the maximum heat flux trajectory, with a maximum flux $\sim$

1064 KW/m^2 found at stagnation point. (turbulent regime applied over the whole surface w.r.t. Reynolds criteria, T_w = 300 K).

- undershoot trajectory corresponding to the maximum energy trajectory.

6.4. Charring Ablation Model and Analysis Code

The materials that we will use (Norcoat-Liège) is a so called charring material, *i.e.* a material that will decompose when subjected to high temperatures. The decomposition of the material will manifest itself by a decrease in material density. In general a material will consist of different constituents, thus degradation of the material can take place over different temperature ranges. To account for this type of behavior, a multi-species Arrhenius definition (as given in [4]) can be used. Here we will only use a single species Arrhenius law due to the material model that is available.

$$\frac{\partial \rho}{\partial t} = -A\rho_v^{1-N}(\rho - \rho_c)^N e^{-\frac{E}{RT}} \tag{1}$$

The degradation of the material will result in the production of gaseous products, and these products will diffuse through the material. The steady state gas mass balance equation is used, resulting in Eq. 2.

$$\frac{\partial \rho}{\partial t} + \nabla.\dot{\overline{m}}^g = 0 \tag{2}$$

We assume a perfect gas law, and we will introduce Darcy's law to relate the pressure of the gas to the gas mass balance, resulting in Eqs. 3-4.

$$\dot{\overline{m}}^g = -K_P \nabla P \tag{3}$$

$$K_P = \frac{M^g \beta P}{\mu^g RT} \tag{4}$$

By introducing the pressure P as a variable, we will be able to define a 3D gas flow, using a scalar degree of freedom. Thus we do not have to impose a direction of gas mass flow before hand. For the heat balance equation, we look at the following phenomena, time variation of the enthalpy (both solid and gas), heat conduction, and the presence of gas in the pores of the solid. The model is set up with a local thermal equilibrium assumption. This means that the gas and the solid have the same temperature at the point scale. With the assumption of linear variation of the enthalpy, we obtain the heat balance equation of Eq. 5.

$$-\frac{\partial \rho}{\partial t} H_p + \rho c \frac{\partial T}{\partial t} = -\nabla.\lambda \nabla T - \dot{\overline{m}}^g.\nabla h^g \tag{5}$$

And the pyrolysis heat will than be defined by Eq. 6.

$$H_p = h^g - \frac{\rho_v h_v - \rho_c h_c}{\rho_v - \rho_c} \tag{6}$$

All the material properties ($\lambda, \rho c$) are obtained by interpolation of the temperature dependent properties between the virgin and the charred state. For this study three types of boundary conditions can be applied to the model. The first will be an applied pressure P on the outer surface, modelling the aerodynamic pressure. The second type of boundary conditions will be the thermal boundary conditions in the form of an applied flux.

$$-\lambda \frac{\partial T}{\partial \overline{n}} = q(T_w, \overline{x}, t) + \epsilon\sigma(T_r^4(\overline{x}, t) - T_w^4) \tag{7}$$

In Eq. 7, the applied flux q will depend on the wall temperature the position along the TPS and the time, while the second term models the (re)-radiation with the environment, The third type of boundary condition is the imposed ablation speed, which in this case is a measured quantity.

$$\dot{s} = \dot{s}(T_w) \tag{8}$$

The surface ablation is implemented by a moving ablation surface and a deforming, in volume, mesh as described in [4]. These equations have been implemented in the Finite Element program SAMCEF. One of the main quantities we are interested in this study, and the main justification for performing a 3D analysis (in this case), is the position of the Center of Gravity of the heat shield. The Center of gravity is defined by Eq. 9.

$$\overline{x}_{c.o.g.} = \frac{\int \rho(\overline{x}, t)\overline{x}\, dV}{\int \rho(\overline{x}, t)\, dV} \tag{9}$$

Within the finite element approach used this position will be automatically calculated and is defined in Eq. 10.

$$\overline{x}_{c.o.g.} = \frac{\sum \int_e \rho(\overline{x}, t)\overline{x}\, dV^e}{\sum \int_e \rho(\overline{x}, t)\, dV^e} \tag{10}$$

6.5. Loads and Boundary Conditions

Within the AEROFAST project two aerocapture geometries have been used, namely an Apollo type shape and a biconic shape. The boundary conditions are a convection flux, that is given as a function of wall temperature (T_w) and time, and an incident radiation flux as a function of time (see Eq. 7). Additionally, for both aerocapture shapes the heat loads are given along the surface ($\overline{x}$). The heat flux that is used, is obtained for a maximum heat load trajectory in a CO_2 atmosphere. In Fig. 24 we show the cold wall (T_w = 300 K) heat flux and radiation temperature, for both aero-shapes, at the stagnation point. These loads will be used to determine the maximum TPS thickness for both shapes.

6.6. 1D Thickness Calculation

For the 1D thickness calculation we use the geometry as given in Fig. 25. The heat shield consists of a honeycomb support structure to which a cork (Norcoat-Liège) material is glued. The honeycomb structure has Carbon Fiber

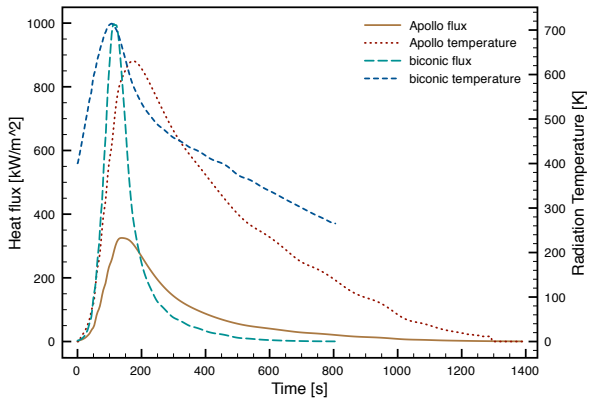

Figure 24. Cold wall flux and radiation temperature at the stagnation point.

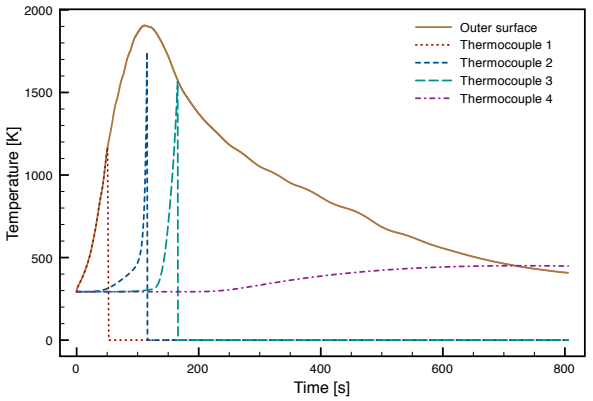

Figure 26. Temperature evolution for the biconic shape at stagnation point load.

Reinforced Plastic outer faces and the honeycomb material itself is made of Aluminium. The thicknesses of all materials are given, except of the cork TPS which has to be determined. In the TPS part, a non-uniform mesh is chosen with a finer distribution close to the loaded surface.

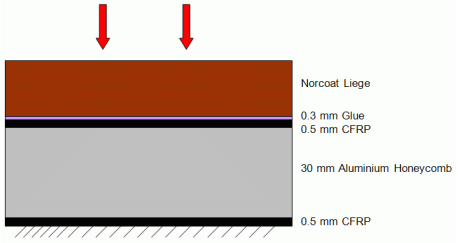

Figure 25. Thermal Protection System plus the support structure.

The initial temperature of the structure equals 293.15 K and the pressure at the outer surface is fixed to 6.10^3 N/m^2 (maximum local pressure near stagnation point). The value of the pressure will not have a influence on the result because no blocking of boundary conditions will be modelled and the thermo-physical properties of the supplied model for the Norcoat-Liège are pressure independent. To determine the thickness of the of the TPS material we define a maximum allowable temperature of the support structure that may not be surpassed during the analysis. The maximum allowable temperature for the Glue will be set to 453 K (180 °C). The heat loads of Fig. 24 will be applied and on the back-side we assume an adiabatic boundary condition. In Fig. 26 and 27 we will show some results for the highest heat load *i.e.* for the biconic case.

In Fig. 26, we see the temperature evolution, in the 1D test-specimen, for different thermo-couple positions through the thickness. The four thermo-couples are placed at respectively $\frac{1}{8}\Delta x$, $\frac{1}{4}\Delta x$, $\frac{1}{2}\Delta x$ and Δx. As can be seen the thermo-couples will loose "signal" when the ablation surface reaches the thermo-couple position. In Fig. 27 we see the density evolution for the same thermo-couples. The density at the outer surface shows that after around 75 seconds the ablation speed is higher than the speed with which the pyrolysis front is moving, resulting in the increase of material density at the outer surface.

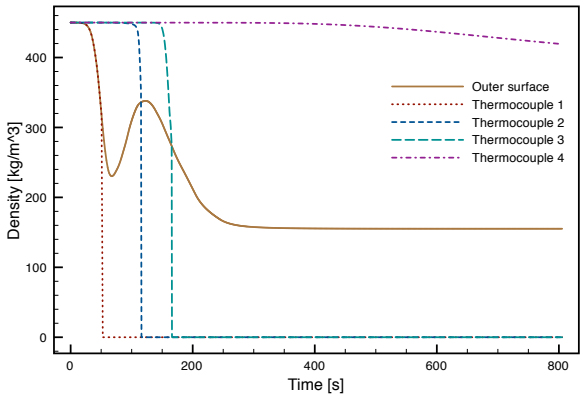

Figure 27. Density evolution for the biconic shape at stagnation point load.

In Fig. 28 the maximum support structure temperature is plotted against the TPS thickness Δx, for both the Apollo and the biconic heat load. It can be seen that the maximum thickness for both aeroshapes is respectively 17 mm for the Apollo shape and 19 mm for the biconic shape.

6.7. 3D TPS Sizing

A total of four different 3D heat shields will be analyses, namely:

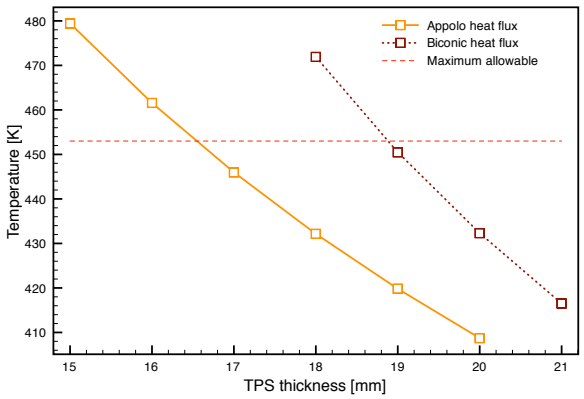

Figure 28. Maximum support temperature as a function of TPS thickness at stagnation point.

- Apollo shape heat shield with a constant thickness of 17 mm.
- A biconic shape with a constant thickness of 19 mm.
- Two variable thickness heat shields with the thickness distributions given in Table 5.

6.7.1. Apollo Type Heat Shield

The Apollo like shape is subjected to the heat flux belonging to the maximum heat load trajectory in a CO_2 atmosphere with a constant bank angle of 180°. In Fig. 29 we see the mass evolution and the Center Of Gravity displacement of the complete heat shield (TPS + support structure). The total mass equals 133.5 kg and the mass loss equals 25.6 kg (see Table 6 for a comparison of aeroshapes).

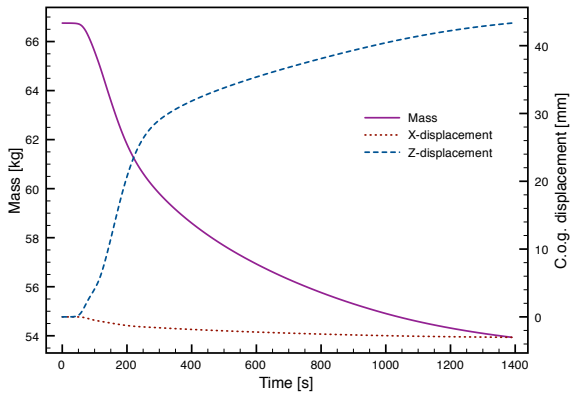

Figure 29. Mass and c.o.g shift for the half heat-shield

In Fig. 30 we see the total ablation deformation on the heat shield at the end of the trajectory.

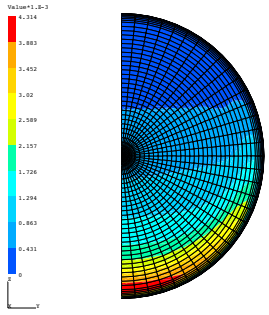

Figure 30. Final ablation deformation.

6.7.2. Bi-conic Shape Heat Shield

The first biconic analysis that will be performed, is with a constant thickness TPS, where the thickness is obtained for the stagnation point (19 mm). The second and third analysis will be with a variable thickness TPS thickness, in order to reduce mass. The layout and thickness of the support structure will be the same for both the Apollo and all the biconic configurations.

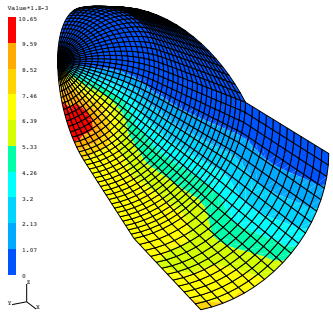

Figure 31. Final ablation deformation.

In Fig. 31 we see the final ablation deformation for the biconic TPS. The total deformation equals 10.6 mm, which is considerably higher than the 4.3 mm of the Apollo like heat shield. In Fig. 32 we show the mass evolution of all three biconic configurations. The total mass of the constant thickness TPS equals 295.4 kg, which is much higher than the Apollo shape shield and considerably over mass budget.

This high mass of the constant thickness TPS prompted the development of a variable thickness TPS. In this case the thickness was calculated, using the same procedure as for the stagnation point, for 10 points around the TPS. These points and given in Fig. 33, and the thickness values are given in Table 5 in the column TPS #1. With the thickness at these points the thickness variation was obtained by linearly interpolating the thickness between the points.

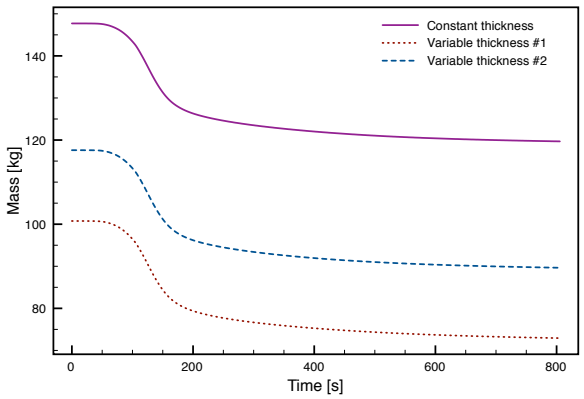

Figure 32. Mass evolution for the half heat-shield

The first constant thickness TPS resulted in an unacceptable design, due to the fact that the maximum support temperature is not respected, as can be seen in Fig. 34. The problem is that the maximum allowable support temperature is respected at the position of the 10 points, but due to the non-linear variation (over the surface) of the external load not in between these points. This resulted in the development of a second variable thickness TPS (TPS #2 in Table 5), for which the temperature distribution on the inside is given in Fig. 35.

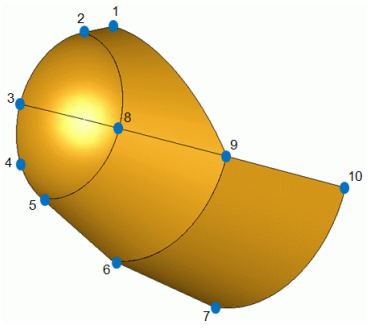

Figure 33. Thickness distribution along the heat-shield.

In Fig. 36 the position of the c.o.g. of the three biconic heat shields are given. The maximum relative (with respect to the shield's diameter) c.o.g. displacements are given in Table 6.

6.8. Results

In Table 6 all the results of the four heat shields are summarized. From these four heat shields the variable thickness TPS #1 is not allowable, while the constant thickness biconic heat shield is too heavy. This leaves the Apollo and variable thickness TPS #2 as acceptable solutions. The maximum allowable relative c.o.g. displacement of

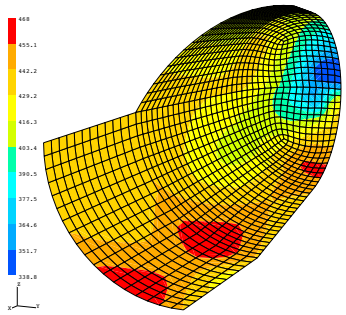

Figure 34. Inner temperature at the end of the trajectory (var. thickness TPS #1).

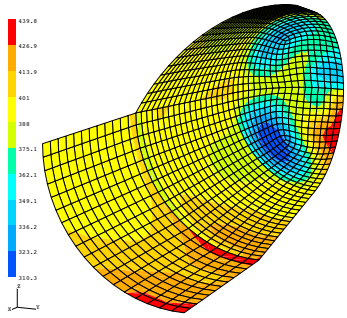

Figure 35. Inner temperature at the end of the trajectory (var. thickness TPS #2).

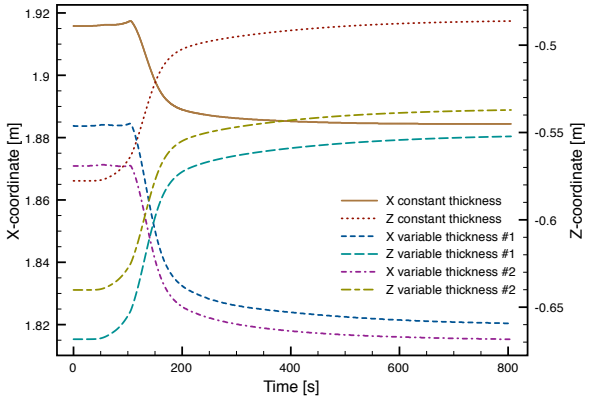

Figure 36. C.o.g position for the half heat-shield

Table 5. Thickness distribution

Point number	S/D [-]	ϕ [°]	TPS #1 [mm]	TPS #2 [mm]
1	0.520	0.00	6	**8**
2	0.381	0.00	6	**8**
3	0.000	180.0	15	15
4	0.212	180.0	19	19
1	0.381	180.0	16	**19**
6	0.798	180.0	16	16
7	1.325	180.0	16	16
8	0.381	90.0	8	**10**
9	0.798	90.0	8	**10**
10	1.325	90.0	7	**10**

approximately 2-3 % is reached, but the results here only include the heat shield and not the rest of the entry vehicle.

Table 6. Mass and c.o.g data for the heat shield.

Heat Shield	Mass [kg]	Mass-loss [kg]	$\frac{x_{c.o.g.}}{D}$ [%]	$\frac{z_{c.o.g.}}{D}$ [%]
Apollo	133.5	25.6	-0.083	0.12
Const. thickness	295.4	56.1	-0.88	2.54
Var. thickness #1	201.6	55.8	-1.76	3.20
Var. thickness #2	235.1	55,8	-1.55	2.86

6.9. Non Ablative Solution Sizing

Considering both families of non ablative material describe in section 5, a preliminary sizing have been performed. In Table 7 the mass optimized TPS pattern for this aerocapture mission is described.

Table 7. Non Ablative TPS heat-shield sizing

Surface zone	Thickness [mm]	Areal weight [kg/m^2]	Mass with 10% margin [kg]
1	2.4 (C/SiC) 21 (IFI)	6.65	19.4
2	2.4 (C/SiC) 19 (IFI)	6.42	44.1
3	2.4 (C/SiC) 18 (IFI)	6.30	23.7
4	2.4 (C/SiC) 7 (IFI)	5.03	37.0
5	2.4 (C/SiC) 6 (IFI)	4.92	31.6
6	6 (F-EI-650)	0.90	10.1

7. CONCLUSIONS

Funded under the 7^{th} Framework Program (FP7) of the European Community, the AEROFAST project has the ambition to remediate to the low level of technology maturity in aerocapture by a demonstration of complete mission study of a Martian aero-capture. This paper described the approach and the preliminary promising results of the development of 2 families of innovative cork based thermal protection material compliant with the specific aerocapture mission requirement. The development of the 3D charring ablation module (Amaryllis) in the finite element code SAMCEF, was also successfully validated and applied for the sizing activities of the different selected aero-shape. In the future, the most promising material candidates should be tested under a larger range of thermal environment in order to qualified the materials for an aerocapture mission but also to improve the thermal and ablative numerical model to take into account for example swelling phenomena or ablation scheme.

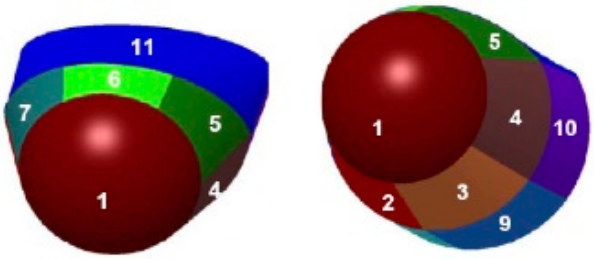

Figure 37. Non Ablative TPS heat shield pattern

REFERENCES

1. T. Salmon, F. Bonnefond, P. Augros, T. Lutz, *AEROFAST: Aerocapture For Futur Space Transportation*, 3^{rd} international ARA days, Arcachon, May 3^{rd} 2011.

2. Jean-Marc Bouilly Bouilly - AST-SAS, *AEROFAST Development of innovative thermal protections*, 3^{rd} international ARA days, Arcachon, May 3^{rd} 2011.

3. Philippe Vernis AST-SAS, *AEROFAST Aerocapture GNC design and performance*, 3^{rd} international ARA days, Arcachon, May 3^{rd} 2011.

4. A.J. van Eekelen, J.-M. Bouilly, S. Hudrisier, J.-M. Dupillier and Y. Aspa. *Design and Numerical Modelling of Charring Material Ablators for Re-entry Applications.* In 6^{th} European workshop on Thermal Protection Systems and hot structures, April 2009, Stuttgart.